(Received 15 April 2026, Accepted 19 May 2026, Scheduled 29 May 2026)

A Compact SRR Metamaterial and DGS-Based Dual-Bandpass Filter for Sub-6 GHz Wireless and IoT Applications

Youssef Khardioui[1,*], Younes Siraj[1], Kaoutar El Bakkar[2], Ali El Alami[1], Mohammed El Ghzaoui[2], and Youssef Mejdoub[3]

[1]*ISMSE Laboratory, Faculty of Sciences and Technology Moulay Ismail University of Meknes, B.P. 509, Boutalamine, Errachidia, Morocco*
[2]*Faculty of Sciences, Sidi Mohamed Ben Abdellah University, Fez, Morocco*
[3]*Laboratory of Networks, Computer Science, Telecommunication & Multimedia (RITM) Higher School of Technology, Hassan II University, Casablanca, Morocco*

ABSTRACT: In modern wireless communication systems, it is essential to use a bandpass filter at the front end of the radio receiver to limit the bandwidth of the signal before it is passed to the rest of the receiver. This study presents the design, fabrication, and analysis of a compact dual-band metamaterial bandpass filter (BPF) for modern wireless communication systems. The proposed structure evolves from an initial open-loop resonator design and integrates metamaterial unit cells to significantly enhance frequency selectivity, reduce insertion loss, and improve impedance matching. To further enhance the performance, defected ground structures were incorporated, resulting in refined bandwidth control and superior return-loss characteristics. The final filter operates at center frequencies of 2.4 and 3.95 GHz, achieving low insertion losses of 0.6 and 0.9 dB, along with return losses of 27.6 and 32.9 dB, respectively. Its compact size of $20 \times 18.46\,\text{mm}^2$ corresponds to an electrical size of $(0.33 \times 0.25)\lambda_g^2$. Owing to its excellent electrical performance and miniaturized form, the proposed filter is suitable for wireless communication applications, including GPS, Bluetooth, Wi-Fi, WiMAX, 5G, and sub-6 GHz bands, making it ideal for modern systems, such as the Internet of Things (IoT).

1. INTRODUCTION

In today's hyper-connected world, wireless communication technologies are the invisible threads weaving our digital fabric. These technologies are evolving at a breakneck speed to keep pace with the demands of the Internet of Things (IoT) and Industry 4.0 [1]. Modern wireless data communication systems necessitate extensive infrastructure development and installation to handle the expanding data streams that traverse next-generation networks [2]. Researchers have focused on discovering, developing, and implementing elements that make the best possible use of the spectrum, such as antennas and filters [3, 4]. The range of wireless communication technologies that have emerged over the last two decades is immense. The most recent development is the design of these elements using metamaterials [5, 6].

Traditional filters in wireless communication systems have limitations in terms of size, performance, and flexibility [7]. However, metamaterial filters are changing the game. The reasons are as follows: Miniaturization: Metamaterial filters can be compact. Enhanced performance: These filters demonstrate superior frequency selectivity and reduced insertion loss [8]. Multi-band operation: They can perform efficiently across multiple frequency bands simultaneously, which is a critical requirement in modern wireless communication systems [9, 10].

In recent years, advanced design methodologies, particularly those employing metamaterial-based concepts, have been extensively investigated to realize innovative and high-performance multiband bandpass filters. For example, [11] presents a novel compact all-frequency absorptive dual-band bandpass filter (BPF) that combines an N-shaped microstrip coupler with T-shaped transmission-line absorption branches. The T-shaped absorptive branches effectively suppress reflected stopband signals across all frequencies, enhancing performance and reducing system complexity. The authors of [12] propose two compact dual-band substrate-integrated waveguide (SIW) bandpass filters using open-loop ring resonators (OLRRs) for enhanced performance. The first filter uses face-to-face OLRRs for miniaturization, achieving a size reduction of over 85%, while the second introduces two horizontally placed resonator units to realize two-pole filtering. Both designs demonstrate low insertion loss (0.85–1.15 dB), high selectivity with transmission zeros, and wide fractional bandwidths (up to 14.9%). Ref. [13] proposes a compact dual-band substrate integrated waveguide (SIW) BPF loaded with complementary split-ring resonators (CSRRs) for C- and X-band applications. By integrating CSRR structures on the SIW surface and optimizing design parameters through a genetic metaheuristic algorithm, their approach achieved two resonant bands at 6.8 GHz and 10.3 GHz with low insertion losses (-1.7 dB and -1.9 dB) and enhanced out-of-band rejection. This work highlighted the effectiveness of metamaterial-inspired unit cells and optimization algorithms in reducing size and improving filter performance. In parallel, [11] introduces

* Corresponding author: Youssef Khardioui (youssef.khardioui@gmail.com).

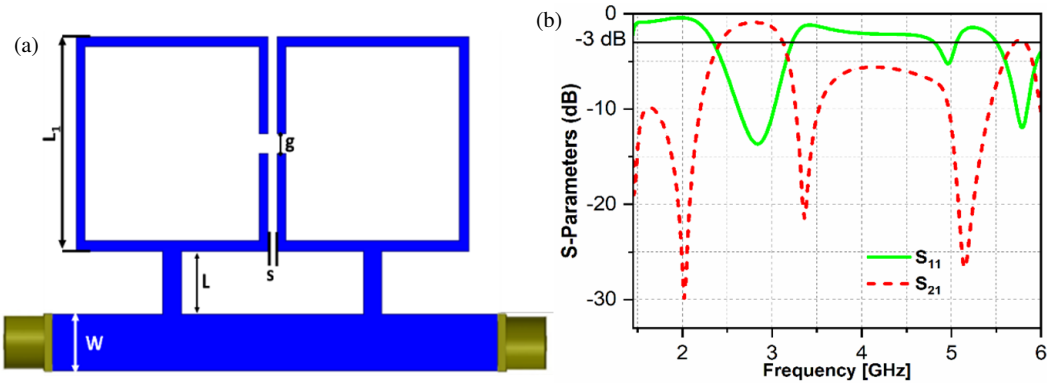

FIGURE 1. (a) Structure of initial BPF. (b) S-parameters results.

an all-frequency absorptive dual-band BPF combining an N-shaped microstrip coupler with T-shaped transmission-line absorption branches. Their structure achieved dual passbands at 1.3 GHz and 4.1 GHz with wide fractional bandwidths (60.5% and 13.3%) and low insertion loss (0.75 dB), while simultaneously absorbing stopband signals to mitigate system reflections. Collectively, these studies highlight the continuous advancement of modern dual-band filter technologies, ranging from SIW-based metamaterial structures to absorption-integrated planar microstrip configurations. These approaches demonstrate various complementary techniques for improving compactness, frequency selectivity, impedance matching, and overall electrical performance in advanced radio frequency (RF) and wireless communication systems. In addition, a dual-band microstrip bandpass filter employing quad-mode stub-loaded resonators is reported in [14] for WLAN applications. The proposed design achieved low insertion loss, good return loss characteristics, enhanced selectivity, and improved isolation between the operating bands.

Compared with previously reported SRR/DGS dual-band filters, the proposed design introduces a compact microstrip configuration that combines metamaterial (MTM) SRR unit cells with Defected Ground Structures (DGSs) to significantly improve the filter performance. The incorporation of MTM cells enhances resonance characteristics and impedance matching, while the DGSs improve selectivity and bandwidth control through generating multiple transmission zeros. As a result, the proposed filter achieves low insertion losses, high return losses, compact dimensions, and excellent dual-band operation using a low-cost FR4 substrate, making it highly suitable for modern IoT and sub-6 GHz 5G wireless communication systems.

This study focuses on the design of a dual-band bandpass filter that evolves through multiple stages. Starting from a conventional open-loop resonator configuration, the design is enhanced by substituting the resonators with metamaterial unit cells and further refined using DGSs. The result is a highly compact and efficient filter suitable for wireless communication standards, such as GPS, Bluetooth, Wi-Fi, WiMAX, 5G, and sub-6 GHz applications, particularly in modern electronic platforms like Internet of Things (IoT) systems and next-generation 5G networks.

The contributions of the proposed work can be outlined as follows:

- A compact dual-band bandpass filter is proposed using MTM unit cells and DGSs.
- It operates at 2.4 and 3.95 GHz, covering key wireless standards, including Bluetooth, WiFi, GPS, WiMAX, and 5G sub-6 GHz.
- Miniaturized structure with a physical size of $20 \times 18.46\,\text{mm}^2$, corresponding to $(0.33 \times 0.25)\lambda_g^2$.
- Fabricated on a low-cost FR4 substrate, with measured results closely matching simulations.
- They are suitable for integration into modern systems, such as IoT devices, 5G terminals, and compact wireless modules.

2. METAMATERIAL BANDPASS FILTER DESIGN APPROACH

This section describes the step-by-step design of a compact bandpass filter (BPF) with a metamaterial-inspired structure. The design is built on an FR4-epoxy substrate and utilizes a split-ring resonator (SRR) unit cell etched directly onto the top metal layer to achieve improved performance in modern wireless systems. The development was structured in three phases: conventional filter design, SRR unit cell definition, and final metamaterial BPF configuration.

2.1. Design of Initial Bandpass Filter

The initial design of the bandpass filter was based on an open-loop resonator topology, as illustrated in Figure 1(a). The structure consists of two open-loop square resonators coupled via a narrow central line. The key geometric parameters that define the filter performance include the resonator length (L_1), feed-line width (w), coupling gap (g), spacing (s), and stub length (L). This microstrip layout provides a compact footprint and is suitable for planar circuit integration.

The simulated S-parameters, shown in Figure 1(b), demonstrate that the filter exhibits dual-band characteristics with center frequencies of 2.8 and 4.08 GHz. The performance at these bands is characterized by insertion losses of 0.92 dB and 5.2 dB, indicating relatively low loss at the first passband and higher attenuation at the second. Return loss values of 13.3 dB at 2.8 GHz and 2.4 dB at 4.08 GHz suggest good impedance matching at the lower band, while the higher band suffers

TABLE 1. Dimensional descriptions for the suggested bandpass filter.

Parameter	L	W	s	g	L_1	L_2	L_3	L_4	W_1
Value (mm)	2.5	2.24	0.46	0.8	8.5	6.9	2.1	1.05	0.4
Parameter	W_2	W_3	d	d_1	M	M_1	a	S_1	
Value (mm)	0.8	0.4	0.4	0.4	1.3	1.12	6.9	2	

from reflection, possibly due to weak coupling or non-optimal impedance transition.

This initial configuration served as a baseline for further improvements. Although the structure achieves a dual-band response, the performance of the second passband, particularly the high insertion loss and poor return loss, necessitates enhancement.

2.2. Metamaterial Unit Cell Design

In microwave communication systems, achieving a multi-band operating frequency requires careful consideration of several design factors. The resonant frequency can be tuned by adjusting the substrate's size and thickness [15, 16]. Other critical parameters play a dominant role. They include the length and width of the ring resonator, the spacing between rings, the gap, and overall ring dimensions. Variations in these parameters directly influence the capacitance and inductance of the structure, thereby affecting its ability to operate in multiple frequency bands.

The geometry of the proposed metamaterial (MTM) unit cell is shown in Figure 2. The structure was realized on an FR4-epoxy dielectric substrate with dimensions of $8.5\times8.5\,\text{mm}^2$ and a thickness of 1.2 mm. The unit cell consists of two split-ring resonators (SRRs) and four quadrilateral V-shaped resonators embedded within. Both the square rings and V-shaped resonators have a uniform width of 0.4 mm. A complete list of the dimensional parameters of the MTM unit cell is provided in Table 1.

To enhance the electromagnetic performance of the proposed design, the structure was optimized using ANSYS HFSS. For the simulation, the incident electromagnetic wave propagates along the Z-axis, whereas the electric and magnetic fields are applied along the X-axis and Y-axis, respectively, to accurately analyze the resonant behavior and frequency response of the unit cell.

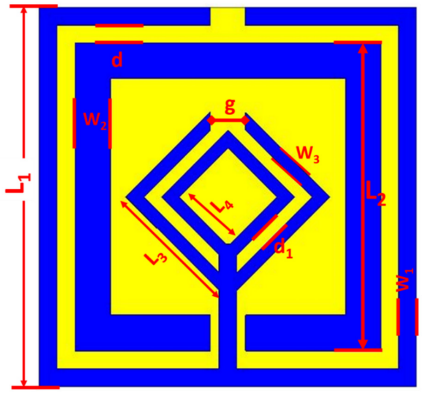

FIGURE 2. Geometry of metamaterial unit cell.

In metamaterials, the electromagnetic properties are often characterized by unusual values of effective permittivity (ε_r), effective permeability (μ_r), and refraction index n_r [4]. Metamaterials are designed to have properties that are not found in natural materials, including negative values for these parameters [17].

The permittivity and permeability were extracted from the S-parameter obtained using the Nicolson-Ross-Weir technique [18, 19]. The effective parameters were determined using Equations (1), (2), and (3) [20, 21].

$$\mu_r = \frac{2}{jK_0h}\frac{1-V_2}{1+V_2} \tag{1}$$

$$\varepsilon_r = \frac{2}{jK_0h}\frac{1-V_1}{1+V_1} \tag{2}$$

$$n_r = \frac{2}{jK_0h}\sqrt{\frac{(S_{21}-1)^2-S_{11}^2}{(S_{21}+1)^2-S_{11}^2}} \tag{3}$$

where h is the thickness of the substrate; k_0 is the wave number; V_1 and V_2 are the composite terms of addition and subtraction of S-parameters respectively, which can be represented by Equations (4) and (5), respectively:

$$V_1 = S_{21} + S_{11} \tag{4}$$

$$V_2 = S_{21} - S_{11} \tag{5}$$

where S_{21} is the transmission coefficients, and S_{11} is the reflection coefficient.

Figure 3 illustrates the real and imaginary components of the permittivity (ε_r), permeability (μ_r), and refractive index (n_r). In Figure 3(a), it is evident that the designed metamaterial (MTM) unit cell exhibits a relative permeability (μ_r) with a real part of approximately 1.72 at 6 GHz and negative peaks reaching values lower than -12. Figure 3(b) presents the relative permittivity (ε_r) as a function of frequency (GHz). The real part of (ε_r) becomes negative at multiple resonance frequencies, specifically at approximately 2 and 4.3 GHz, indicating strong dispersive behavior. Similarly, the refractive index (n_r) demonstrates negative values within several frequency bands: from 1 to 2.1 GHz and 4.3 to 6 GHz as shown in Figure 3(c). These negative regions confirm the metamaterial properties of the proposed unit cell, demonstrating its ability to support left-handed wave propagation. Additionally, the effective refractive index (n_r) curve exhibits a region where the real part of the index approaches zero, indicating near-zero index behavior. This near-zero refractive index (NZI), which may arise from

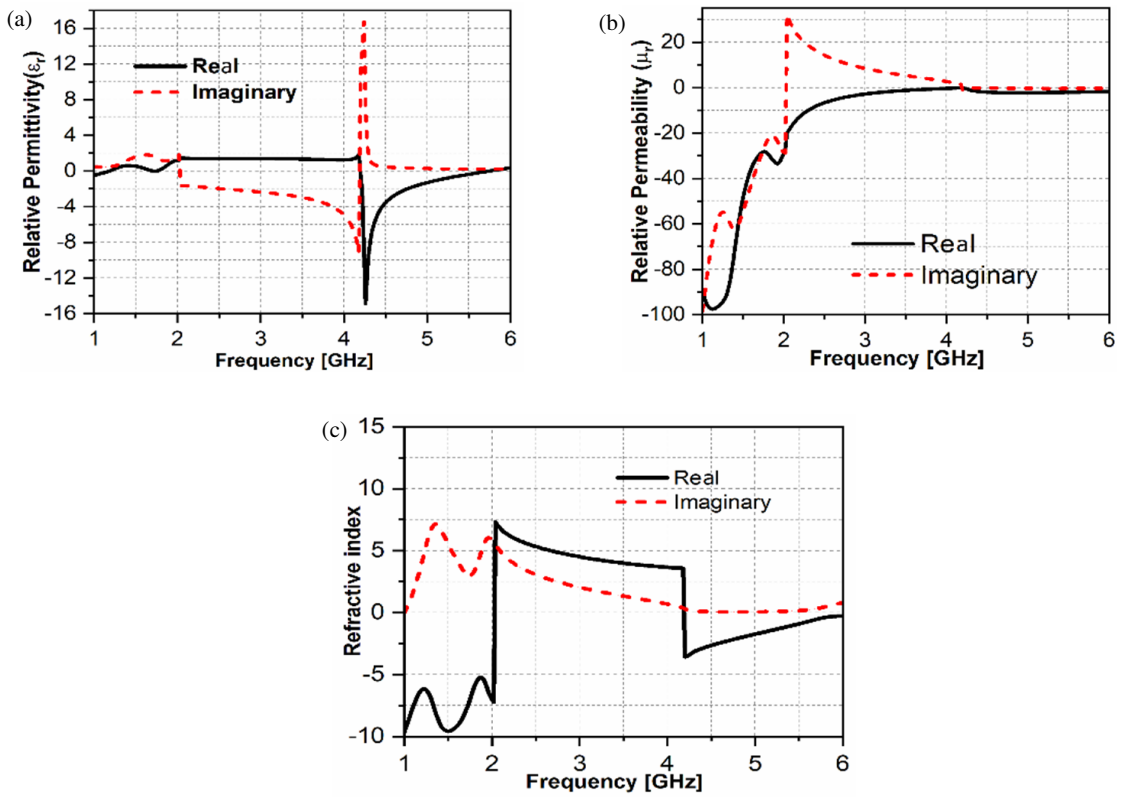

FIGURE 3. (a) Relative permeability. (b) Relative permittivity. (c) Refractive index.

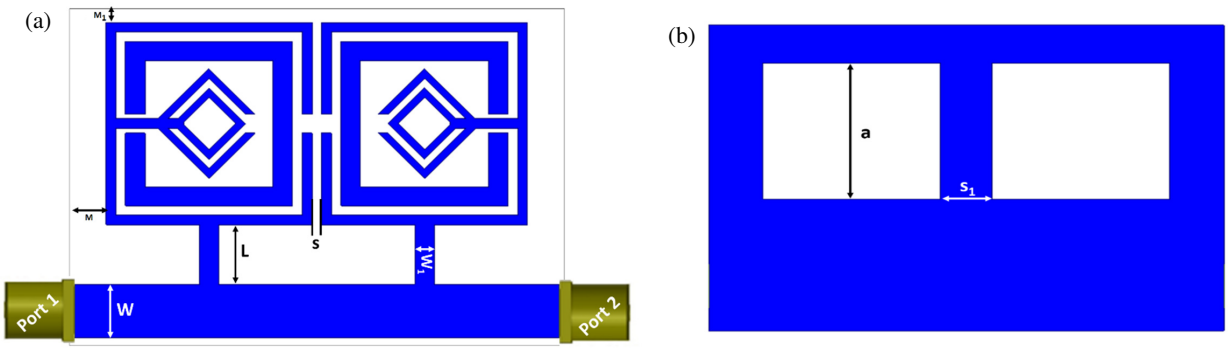

FIGURE 4. Geometry of the proposed bandpass filter: (a) Top View. (b) Bottom View.

epsilon-near-zero (ENZ), mu-near-zero (MNZ), or index-near-zero (INZ) conditions, enables unusual electromagnetic properties, such as uniform phase distribution, infinite phase velocity, and the ability to tunnel electromagnetic energy through narrow or sharply bent waveguides.

2.3. Metamaterial Bandpass Filter Design

To enhance the performance of the initial bandpass filter, the conventional open-loop square resonators were replaced by two MTM unit cells, resulting in a significantly improved filter structure. This novel design is illustrated in Figure 4, which highlights the top and bottom metallization along with the compact dimensions of the proposed configuration. The parameter dimensions in the filter are presented in Table 1.

The integration of MTM cells contributes to enhanced electromagnetic behavior due to their engineered negative effective permittivity and/or permeability and a near-zero index behavior. These cells introduce additional degrees of freedom in filter design, enabling improved control over resonance characteristics and coupling effects.

The updated filter exhibits center frequencies at 2.38 GHz and 4.4 GHz, as observed in the S-parameter results shown in Figure 5. These frequencies are close to the targets of the original design but offer significantly better performance. Notably, the insertion losses are reduced to 0.68 dB and 1.1 dB at the respective bands, indicating more efficient transmission. The return losses are also substantially improved, reaching 20.36 dB at 2.38 GHz and 31.1 dB at 4.4 GHz. These values reflect ex-

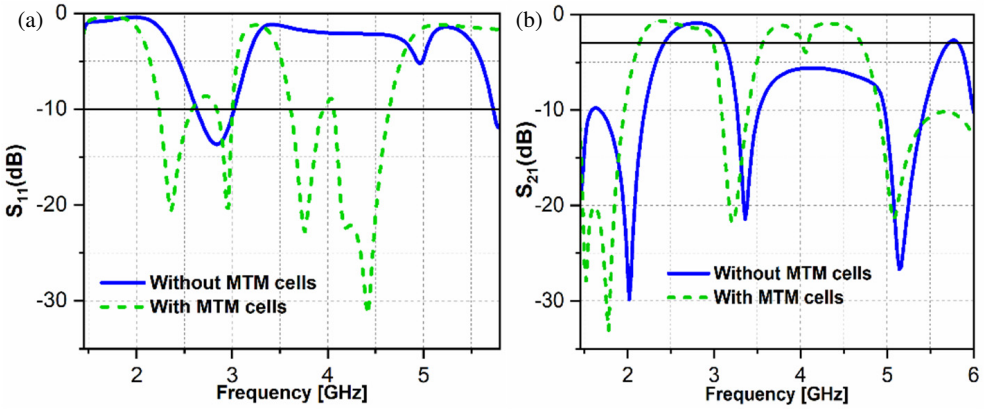

FIGURE 5. S-parameters results for initial and metamaterial BPF: (a) S_{11}, (b) S_{21}.

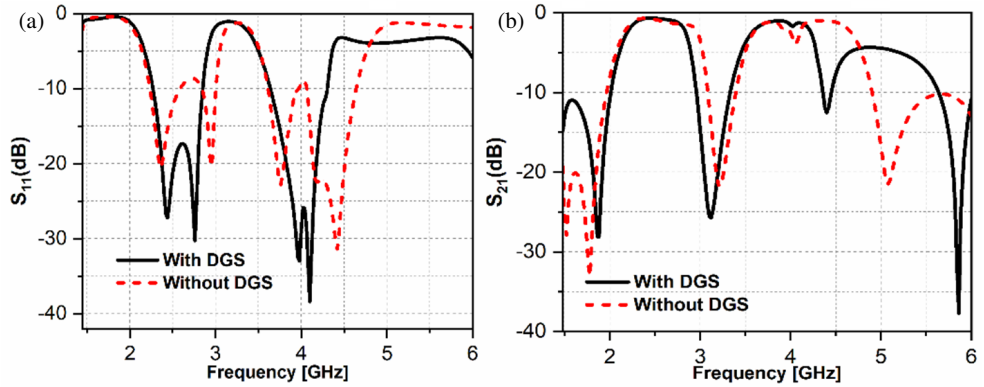

FIGURE 6. S-parameters of the metamaterial filter with/without DGS.

cellent impedance matching across both passbands, a clear improvement over the initial filter.

To further refine the filter characteristics, two square-shaped defected ground structures (DGSs) were introduced beneath the resonator arms, as illustrated in Figure 6. The inclusion of DGS elements modifies the ground current distribution and introduces additional resonance and filtering effects on the signal. This modification leads to a more compact and sharper frequency response curve.

The final filter configuration achieves center frequencies of 2.4 and 3.95 GHz. The return losses were significantly improved, reaching 27.6 and 32.9 dB, respectively. Moreover, the -3 dB bandwidths are reduced to 0.68 and 0.51 GHz, respectively, indicating narrower and more selective passbands. This refinement results in very low insertion losses of 0.6 and 0.9 dB, respectively, which confirms the high transmission quality of the final design.

The final structure maintains a compact form factor of $20 \times 18.46\,\text{mm}^2$, corresponding to an electrical size of $(0.33 \times 0.25)\lambda_g^2$, where λ_g is the guided wavelength at 2.4 GHz. Overall, the use of metamaterial unit cells, in combination with DGS, leads to a high-performance dual-band filter with excellent impedance matching, reduced bandwidth, and minimal insertion loss, making it ideal for compact RF and microwave applications.

3. THE BANDPASS FILTER RESULTS AND DISCUSSION

3.1. Insertion Loss and Return Loss

Figure 7 presents the simulated S-parameter results of the proposed metamaterial bandpass filter, confirming its effective dual-band operation. The filter exhibits passbands centered at 2.4 and 3.95 GHz. At these frequencies, the return losses $|S_{11}|$ reached 27.6 dB and 32.9 dB, respectively, indicating excellent impedance matching. The corresponding -3 dB bandwidths are 0.68 GHz (ranging from 2.17 to 2.85 GHz) and 0.51 GHz (from 3.5 to 4.24 GHz), with low insertion losses $|S_{21}|$ of 0.6 and 0.9 dB, respectively.

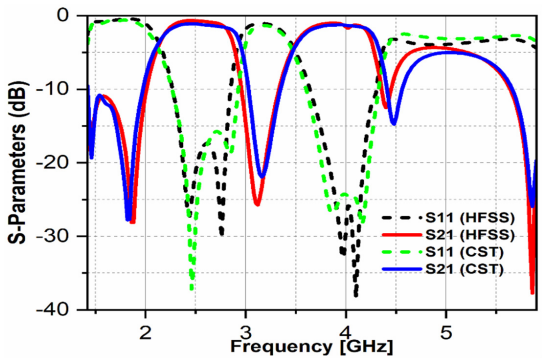

FIGURE 7. S-parameters of the metamaterial bandpass filter.

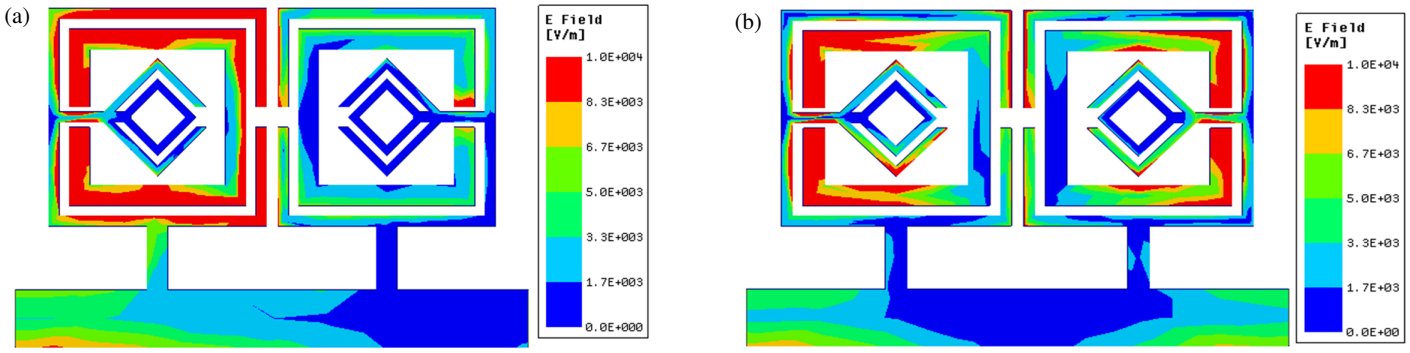

FIGURE 8. E-field distribution at: (a) 2.4 GHz, (b) 3.95 GHz.

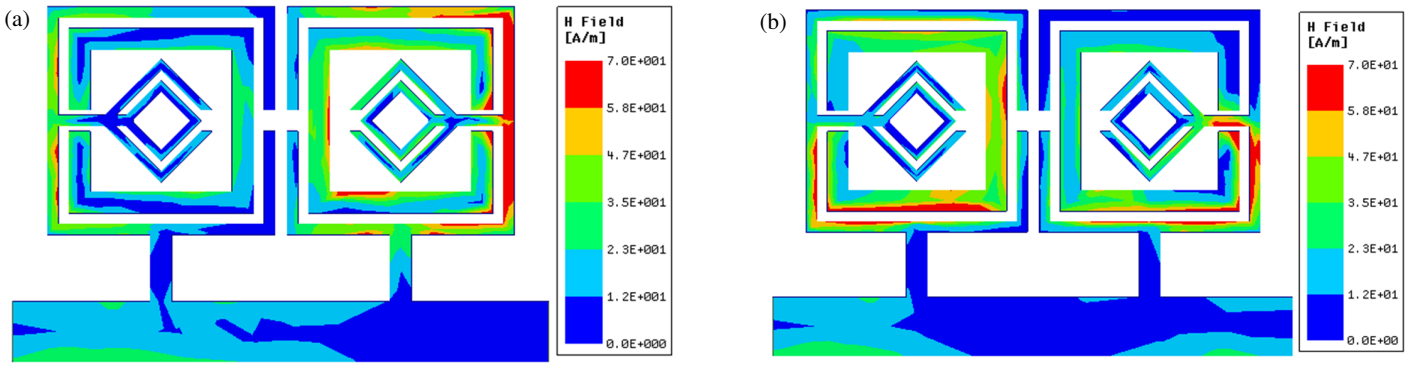

FIGURE 9. H-field distribution at: (a) 2.4 GHz, (b) 3.95 GHz.

Furthermore, the filter demonstrates the presence of four transmission zeros (TZs) strategically placed around the passbands at 1.86 GHz, 3.12 GHz, 4.4 GHz, and 5.86 GHz. These TZs contribute to improved selectivity and out-of-band rejection, thereby enhancing the overall filter performance.

The simulation results confirm that the proposed metamaterial filter is well-suited for multi-band wireless communication systems, particularly those operating in the GPS (2.4 GHz), WiMAX (3.5 GHz), WLAN, and sub-6 GHz 5G (3.5–3.8 GHz) bands.

3.2. Electric and Magnetic Fields Distribution

The concepts of electric and magnetic fields are also essential for understanding the autonomous propagation of electromagnetic waves. The electrical field distributions of the bandpass filter designed at 2.4 GHz and 3.95 GHz are shown in Figure 8(a) and Figure 8(b). The filter shows the maximum distribution (indicated in red) of the electric field between the two square rings of the unit cell at 2.4 GHz, and for the second frequency 3.95 GHz, as shown in Figure 8(b), the maximum distribution of the electric field is observed in the vicinity of all the gaps in the cells.

Figure 9(a) and Figure 9(b) present the H-field distribution of the bandpass filter designed for 2.4 GHz and 3.95 GHz operations. The designed bandpass filter showed the maximum magnetic field H of the first square ring of the cell, for both 2.4 GHz and 3.95 GHz frequencies.

3.3. Validation Experimental

To validate the simulated performance of the proposed metamaterial-based bandpass filter, a physical prototype was fabricated, as shown in Figure 10(b). The filter was implemented on an FR4 substrate, which is widely adopted in printed circuit board (PCB) fabrication due to its low cost and practical availability. The substrate had a dielectric constant of $\varepsilon_r = 4.4$, a thickness of 1.6 mm, and a loss tangent of approximately 0.02. Although FR4 introduces higher dielectric and conductor losses than high-end materials, such as Rogers, it remains a practical choice for prototyping and low-cost wireless applications.

The fabricated prototype of the proposed bandpass filter was experimentally characterized to validate its simulated performance. It is illustrated in the measured S-parameter results shown in Figures 10(a) and 10(b). The filter exhibits two well-defined passbands centered at 2.42 and 3.68 GHz, which are in close agreement with the simulated resonant frequencies. The measured resonant frequencies exhibit slight shifts compared to the simulated results, mainly due to fabrication tolerances, variations in the dielectric properties of the FR4 substrate, and SMA connector/soldering effects.

In terms of transmission characteristics, the measured insertion losses were approximately 0.9 dB at 2.42 GHz and 1.2 dB at 3.68 GHz, which are close to the simulated values of 0.6 and 0.9 dB, respectively. The return losses were approximately 22.8 dB and 36 dB, respectively, which were consistent with the predicted performance. These results demonstrate that the fil-

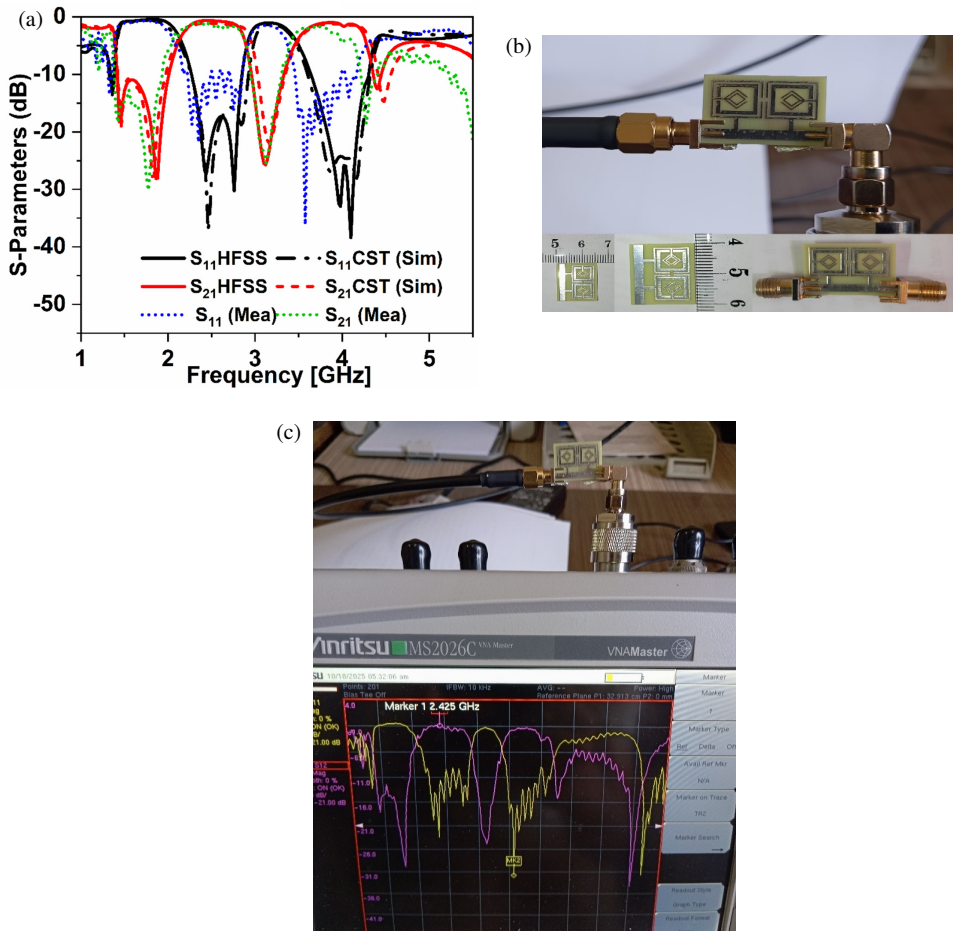

FIGURE 10. (a) Comparison of experimental and simulated S-parameters. (b) Photo of the prototype of the manufactured filter. (c) Measurement setup with VNA.

TABLE 2. A comparison with other published work.

Ref.	f_1/f_2 (GHz)	Technology	FBW (%)	Return loss $\lvert S_{11}\rvert$ (dB)	Insertion loss $\lvert S_{21}\rvert$ (dB)	Size (λ_g^2)
[11]	1.3/4.1	Microstrip	60.5/13.3	> 10	0.75/2.2	0.41×0.20
[12]	1.75/4.65	Microstrip	14.9/10.4	14/21	1.1/1.15	0.041
[22]	2.4/5.2	Microstrip	51.9/23.3	22.1/20.8	0.3/0.7	0.28×0.2
[14]	2.4/5.2	Microstrip	14.8/12.9	10/10	1.43/1.34	0.57×0.13
[23]	4.1/4.93	Coaxial	2.54/3	> 20	0.54/0.34	$0.65 \times 0.3 \times 0.44$
[24]	6.0/9.0	SIW	4.33/4.66	> 25	-	0.44×0.58
[13]	6.8/10.3	SIW	20/55	24/22	1.7/1.9	0.015×0.012
This work	**2.4/3.95**	**Microstrip**	**28.3/12.9**	**27.6/329**	**0.6/0.9**	$\mathbf{0.33 \times 0.25}$

ter maintains excellent impedance matching and low-loss transmission in both passbands, even with the use of FR4 (see Figure 10(c)).

As indicated in Table 2, the proposed metamaterial-based bandpass filter demonstrates superior performance to existing designs in the literature. It achieves lower insertion losses (0.6 dB/0.9 dB) and higher return losses (27.6 dB/32.9 dB) while maintaining a compact size ($20 \times 18.46\,\text{mm}^2$). Unlike many filters that require high-end substrates, this design uses a low-cost FR4 without compromising performance. The inclusion of multiple transmission zeros enhances the selectivity, further distinguishing it from conventional filters. These advantages make the filter highly suitable for GPS, WiFi, WiMAX, 5G sub-6 GHz, and IoT applications.

4. CONCLUSION

In this study, a compact metamaterial-based dual-band bandpass filter was successfully designed, manufactured, and analyzed for modern communication systems. The progression from conventional open-loop resonators to metamaterial unit cells has allowed significant improvements in transmission efficiency and impedance matching. The integration of defected ground structures (DGSs) further enhances the filter performance by improving the return loss and narrowing the bandwidth for better selectivity.

The final filter achieves dual-band operation at 2.4 and 3.95 GHz with low insertion losses of 0.6 and 0.9 dB, respectively, and excellent return losses of 27.6 and 32.9 dB, respectively. The proposed design also features a compact size of $20 \times 18.46\,\text{mm}^2$, corresponding to $(0.33 \times 0.25)\lambda_g^2$, making it highly suitable for integration into space-constrained devices. Given its high performance and small footprint, the proposed filter is a strong candidate for applications in GPS, Bluetooth, Wi-Fi, WiMAX, 5G, and sub-6 GHz communication systems, especially within IoT devices and emerging 5G networks.

REFERENCES

[1] Soori, M., B. Arezoo, and R. Dastres, "Internet of Things for smart factories in Industry 4.0, a review," *Internet of Things and Cyber-Physical Systems*, Vol. 3, 192–204, 2023.

[2] Chen, B., J. Wan, L. Shu, P. Li, M. Mukherjee, and B. Yin, "Smart factory of Industry 4.0: Key technologies, application case, and challenges," *IEEE Access*, Vol. 6, 6505–6519, 2017.

[3] Udhayanan, S. and K. Shambavi, "Compact single notch UWB bandpass filter with metamaterial and SIW technique," *Progress In Electromagnetics Research Letters*, Vol. 117, 41–46, 2024.

[4] Marqués, R., F. Martín, and M. Sorolla, *Metamaterials with Negative Parameters: Theory, Design, and Microwave Applications*, Wiley Series in Microwave and Optical Engineering, Wiley-Interscience, Hoboken, NJ, 2008.

[5] Cui, T. J., D. Smith, and R. Liu, *Metamaterials: Theory, Design, and Applications*, Springer, New York, 2010.

[6] Troudi, Z. and L. Osman, "Analysis and design of band-pass filter based on metamaterial," in *2019 IEEE 19th Mediterranean Microwave Symposium (MMS)*, 1–4, Hammamet, Tunisia, 2019.

[7] Jindal, S. and J. Sharma, "Review of metamaterials in microstrip technology for filter applications," *International Journal of Computer Applications*, Vol. 54, No. 3, 48–54, Sep. 2012.

[8] Yan, S., J. Bao, I. Ocket, B. Nauwelaers, and G. A. E. Vandenbosch, "Metamaterial inspired miniaturized SIW resonator for sensor applications," *Sensors and Actuators A: Physical*, Vol. 283, 313–316, Nov. 2018.

[9] Crnojević-Bengin, V., *Advances in Multi-band Microstrip Filters*, Cambridge University Press, 2015.

[10] Jarry, P. and J. Beneat, *Advanced Design Techniques and Realizations of Microwave and RF Filters*, John Wiley & Sons, Hoboken, NJ, 2008.

[11] Wu, B., K. Song, L. Wang, L. Yi, S. Li, Y. Li, K. Zhu, Y. Cai, W. Zou, and F. Liu, "A compact all-frequency absorptive dual-band bandpass filter with T-shaped transmission line absorption branches," *AEU — International Journal of Electronics and Communications*, Vol. 177, 155228, Apr. 2024.

[12] Pradhan, N. C., S. Koziel, R. K. Barik, A. Pietrenko-Dabrowska, and S. S. Karthikeyan, "Miniaturized dual-band SIW-based bandpass filters using open-loop ring resonators," *Electronics*, Vol. 12, No. 18, 3974, Sep. 2023.

[13] Akkader, S., H. Bouyghf, A. Baghdad, A. K. Belbachir, and M. El Bakkali, "Fabrication of compact substrate integrated waveguide dual band bandpass filter using complementary split-ring resonators for C and X band applications," *e-Prime — Advances in Electrical Engineering, Electronics and Energy*, Vol. 9, 100739, Sep. 2024.

[14] Weng, M.-H., C.-Y. Huang, S.-W. Dai, and R.-Y. Yang, "An improved stopband dual-band filter using quad-mode stub-loaded resonators," *Electronics*, Vol. 10, No. 2, 142, Jan. 2021.

[15] Islam, M. R., M. T. Islam, M. S. Soliman, M. H. Baharuddin, K. Mat, A. M. Moubark, and S. H. A. Almalki, "Metamaterial based on an inverse double V loaded complementary square split ring resonator for radar and Wi-Fi applications," *Scientific Reports*, Vol. 11, No. 1, 21782, Nov. 2021.

[16] Islam, M. R., M. T. Islam, M. Moniruzzaman, M. Samsuzzaman, and H. Arshad, "Penta band single negative meta-atom absorber designed on square enclosed star-shaped modified split ring resonator for S-, C-, X- and Ku-bands microwave applications," *Scientific Reports*, Vol. 11, No. 1, 8784, 2021.

[17] Narayan, S. and A. Kesavan, *Handbook of Metamaterial-derived Frequency Selective Surfaces*, Springer Singapore, Singapore, 2022.

[18] Luukkonen, O., S. I. Maslovski, and S. A. Tretyakov, "A stepwise Nicolson-Ross-Weir-based material parameter extraction method," *IEEE Antennas and Wireless Propagation Letters*, Vol. 10, 1295–1298, 2011.

[19] Edries, M., H. A. Mohamed, S. S. Hekal, M. A. El-Morsy, and H. A. Mansour, "A new compact quad-band metamaterial absorber using interlaced I/square resonators: Design, fabrication, and characterization," *IEEE Access*, Vol. 8, 143 723–143 733, 2020.

[20] Lim, T.-C., *Mechanics of Metamaterials with Negative Parameters*, Springer Singapore, Singapore, 2020.

[21] Ajewole, B., P. Kumar, and T. Afullo, "I-shaped metamaterial using SRR for multi-band wireless communication," *Crystals*, Vol. 12, No. 4, 559, Apr. 2022.

[22] Liang, G.-Z. and F.-C. Chen, "A compact dual-wideband bandpass filter based on open-/short-circuited stubs," *IEEE Access*, Vol. 8, 20 488–20 492, 2020.

[23] Li, C., F.-C. Chen, J.-J. Yan, and R.-C. Lin, "In-line dual-band bandpass filter with multiple transmission zeros based on triplet and strongly coupled resonator pairs," *AEU — International Journal of Electronics and Communications*, Vol. 192, 155696, Mar. 2025.

[24] Chu, P., M. Luo, W. Zhang, F. Zhu, L. Liu, and K. Wu, "Dual band dual mode substrate integrated waveguide filter with mixed coupling," *IEEE Microwave and Wireless Technology Letters*, Vol. 34, No. 11, 1239–1242, Nov. 2024.